PRAMANA
— journal of
physics

Vol. 73, No. 4
October 2009
pp. 765–780

Structural and magnetic properties of size-controlled $Mn_{0.5}Zn_{0.5}Fe_2O_4$ nanoparticles and magnetic fluids

RUCHA DESAI[1], VIPUL DAVARIYA[1], KINNARI PAREKH[2,4,*] and RAMESH V UPADHYAY[3]

[1]Department of Physics, Bhavnagar University, Bhavnagar 364 002, India

[2]Department of Physics, Indian Institute of Technology Gandhinagar, Gandhinagar, India

[3]Charotar Institute of Applied Sciences, Education Campus-Changa, Changa 388 421, India

[4]Permanent address: Department of Physics, Faculty of Sciences, M.S. University of Baroda, Vadodara 390 002, India

*Corresponding author. E-mail: pkinnarih@yahoo.com

MS received 7 October 2008; revised 27 April 2009; accepted 23 May 2009

Abstract. $Mn_{0.5}Zn_{0.5}Fe_2O_4$ ferrite nanoparticles with tunable Curie temperature and saturation magnetization are synthesized using hydrothermal co-precipitation method. Particle size is controlled in the range of 54 to 135 Å by pH and incubation time of the reaction. All the particles exhibit super-paramagnetic behaviour at room temperature. Langevin's theory incorporating the interparticle interaction was used to fit the virgin curve of particle magnetization. The low-temperature magnetization follows Bloch spin wave theory. Curie temperature derived from magnetic thermogravimetric analysis shows that Curie temperature increases with increasing particle size. Using these particles magnetic fluid is synthesized and magnetic characterization is reported. The monolayer coating of surfactant on particle surface is confirmed using thermogravimetric measurement. The same technique can be extended to study the magnetic phase transition. The Curie temperature derived using this measurement complies with the low-temperature magnetic measurement. The room-temperature and high-temperature magnetization measurements are also studied for magnetic fluid systems. The magnetic parameters derived for fluid are in good agreement with those obtained for the particle system.

Keywords. Nanomagnetic particles; superparamagnetism; magnetic fluid; hydrothermal synthesis.

PACS Nos 75.50.Tt; 75.20.-g; 75.75.+a; 81.07.-b

1. Introduction

Tailor-made magnetic ferrite compounds are the subject of recent research due to its wide applications in the domain of nanostructure materials [1–5]. However,

the greatest revolution in this interdisciplinary field has been promoted by developing new measuring techniques and refining synthesis methods, which allow the preparation of particles at the nanometer scale. One of the main features of the nanomaterials is the fact that their microscopic structure – which results from the synthesis method – largely affects the macroscopic properties, giving rise to a wide variety of new phenomena. Among various physical and magnetic properties of nanoferrites, high value of room-temperature magnetization and low Curie temperature (between 300 and 400 K) have attracted many researchers due to its technological importance [6,7]. Moreover, to tune these specific properties at large scale synthesis is a challenging task as the variation in composition or synthetic route and/or synthesis parameters like pH, digestion time, digestion temperature, etc. modify these properties significantly. Keeping these challenges in our mind, in the present paper, we have focussed the synthesis of nanoparticles with tunable saturation magnetization and Curie temperature for large scale synthesis.

The present work is devoted to tailor the microstructure at the nanometric scale and correlate it to the macroscopic properties. Some of these properties, viz. X-ray diffraction, magnetization, AC susceptibility and thermal measurements are discussed in the text. The sample chosen for the study is zinc-doped manganese ferrite ($Mn_{0.5}Zn_{0.5}Fe_2O_4$) because its magnetic properties can be modified significantly either with size or with different site occupancy. Three different sized particles were prepared by controlling synthesis parameters.

2. Methodology

In inverse spinel $Fe_A^{3+}[Me_B^{2+}Fe_B^{3+}]O_4$ with $Me^{2+} = Co^{2+}$, Ni^{2+}, Fe^{2+} and Cu^{2+}, all divalent metal ions occupy octahedral (B) sites and Fe^{3+} ion is distributed on both tetrahedral (A) and octahedral (B) sites. Due to the presence of strong AB and BB interactions (∼10 times) compared to AA interactions, Curie temperature varies between 728 and 858 K for such systems. According to Gilleo [8], the Curie temperature (T_C) is proportional to the number of active magnetic linkages per magnetic ion per formula unit. This model suggests that T_C can change only with the change in the number of magnetic linkages with substitution and not with its character. Consequently, it is valid only when all magnetic ions are identical or when the substituent ion displaces a magnetic ion on the same site. Generally, in substituted ferrimagnetic spinel compound, there exist varying numbers of linkages of different strength. Therefore, one has to take into account this factor while calculating the Curie temperature. Considering this, the Curie temperature, T_C, thus depends on the respective exchange integral J, number of nearest exchange coupled neighbours, n_{ij}, respective divalent metal ion Me and the absolute spin value $|S|$ as given by Groenou *et al* [9],

$$\begin{aligned} T_C \approx \left(\frac{2}{3}k_B\right)[n_{AB}n_{BA}]^{0.5}|S(Fe^{3+})||S(Fe^{3+})|J_{AB}(Fe^{3+}-Fe^{3+}) \\ +[n_{AB}n_{BA}]^{0.5}|S(Fe^{3+})||S(Me^{2+})| \times J_{AB}(Fe^{3+}-Me^{2+}) \\ +[n_{BB}]|S(Fe^{3+})||S(Me^{2+})| \times J_{BB}(Fe^{3+}-Me^{2+}). \end{aligned} \quad (1)$$

Here, k_B is the Boltzmann constant. According to eq. (1), T_C strongly depends on the degree of inversion in the system, the number of nearest exchange coupled neighbours and the absolute spin moment. Thus the Curie temperature of Mn-ferrite is found low (585 K for bulk sample) compared to Fe_3O_4 (858 K). This is because $MnFe_2O_4$ is a partially inverse ferrite system. 80% of the Mn^{2+} ions occupy the A-site and the remaining 20% occupy the B-site of the lattice. As a result, the Fe_A^{3+}–Fe_B^{3+} exchange interaction is replaced by the factor 2 weaker Mn_A^{2+}–Fe_B^{3+} interaction. Here interaction between the ions on the B sites is neglected. The substitution of diamagnetic ions like Zn^{2+} and Cd^{2+} in $MnFe_2O_4$ system will further weaken the J_{AB} interactions which results in the reduction in T_C. However, the saturation magnetization at 0 K, which is the difference between the net magnetic moment of the two sites increases with substitution of non-magnetic ions, provided non-magnetic ion occupies A site. The limit to observe the increase in saturation magnetization and decrease in T_C depends upon the concentration of diamagnetic substitution and the surrounding metal ions in spinel ferrites. It is found from literature that for $x = 0.5$, i.e., $Mn_{0.5}Zn_{0.5}Fe_2O_4$ has the highest value of saturation magnetization in the Zn-substituted Mn ferrite, then onwards by increasing the Zn substitution the saturation magnetization decreases [10]. Hence for the present study the $x = 0.5$ concentration is chosen and the optimization of M_S and T_C has been carried out by changing different synthesis parameters.

3. Experimental section

3.1 *Synthesis of $Mn_{0.5}Zn_{0.5}Fe_2O_4$ nanoparticles and magnetic fluid elaboration*

The magnetic fluid preparation is carried out in three basic steps: (i) synthesis of ferrite nanoparticles, (ii) surface treatment and (iii) suspension of particles to have a stable colloidal solution. Ferrite nanoparticles are prepared using chemical co-precipitation technique followed by hydrothermal route. All the reagents were of analytical grade. The salt solution (pH $<$ 2) of MCl–$FeCl_3$ (M = Mn and Zn) mixed with alkali solution at 305 K under vigorous stirring, leads to a brown coloured precipitation. Since pH, temperature and digestion time, t_d, of the precipitates play crucial roles to control the size of particles, different sized particles were achieved by controlling pH and t_d. For sample A, pH was adjusted to 10.5 and then the precipitate was homogenized for 10 min. Later, the beaker containing the precipitate was transferred to autoclave (NOVA Autoclave Sterilizer, Model No. 8533), which was pre-heated at 323 K. The solution was digested for 30 min at an inert pressure of 15 psi/inch^3 and a temperature of 378 ± 5 K. After the stipulated digestion time (t_d), the inert pressure of autoclave was released, and temperature was lowered down to 323 K. The black precipitate was stirred for 30 min at 303 K. Impurities of sulphate and chloride complexes were removed by giving 300 ml hot distilled water wash (three times), and the supernatant was removed by magnetic decantation. The aliquot of particles were washed with acetone and particles were dried in air for characterization.

Similarly, sample B was prepared at pH 11.6 and digestion time (t_d) 30 min, and sample C was prepared at pH 11.6 and digestion time (t_d) 60 min.

To modify the surface of the above-synthesized nanoparticles, 6 ml of oleic acid was added under constant stirring and homogenized for 1 h at 303 K. The mixture was heated to 363 K for 3–4 min with a heating rate of 3°/min. At this temperature, sodium oleate disintegrates and oleate ions bind chemically on the surface of nanoparticles. After cooling down to an ambient temperature, the coated particles were peptized with diluted (0.01 M) hydrochloric acid. The unreacted/free oleate ions were removed by washing the coated particles with warm distilled water. Acetone wash was given to remove water molecules from the surface of the particles. Finally, acetone wet slurry was divided into two parts. One part was dispersed in 8 ml kerosene and the other in 2 ml diester. Kerosene-based magnetic fluid was prepared by evaporating acetone at moderately high temperature with constant stirring. Slow heating rate was carefully maintained so as to prevent simultaneous evaporation of kerosene. For diester-based magnetic fluid, the secondary stabilizer RE-610 was used to make the oleic acid-coated particles compatible with carrier matrix. All these magnetic fluids were centrifuged at 12,000 rpm for 20 min. The stability of the fluid thus prepared is very high even under gradient magnetic field of 10 kOe.

4. Results and discussion

4.1 *Nanomagnetic particles*

4.1.1 *Structural characterization*

The X-ray diffraction pattern recorded using Bruker X-ray diffractogram model D8 advanced ($\lambda = 1.5414$ Å) shows a single phase cubic spinel structure with no other impurity phases (figure 1). The broadness of all peaks indicates a typical characteristic of nanosize particles. Enhancements in intensity of peaks from sample A to B and B to C reveal that crystallinity increases with increasing pH and digestion time (t_d). The detailed pattern analysis has been carried out using Rietveld refinement program – DBWS-9006 PC, developed by Dr H Marciniat, Poland. The structure model and initial structure parameters taken were: space group Fd3m; metal and iron atoms were in the Wyckoff 8a and 16d special position and O atoms in the 32e special positions. Diffraction profiles were modelled using a multi-term Simpson's rule integration of the pseudo-Voigt function. The quality of fitting is confirmed using the goodness of fit, χ^2 (must be between 1 and 2) and reliability factors, R_p and R_{wp} (weighted differences between measured and calculated values). Because of the similar structure factor of Mn^{2+} and Fe^{3+}, it is assumed that Mn^{2+} resides in tetrahedral (A) site and the remaining ions distributed in A and B sites. The obtained best-fit values are reported in table 1. It is observed from table 1 that 40% zinc ions occupy the tetrahedral (A) site and 60% occupy the octahedral (B) site for sample A, while for samples B and C the zinc ions reside completely on A-site. Lattice parameters (a) obtained from the Rietveld fitting for samples A, B and C are 8.4495 ± 0.0001, 8.4427 ± 0.0001 and 8.4542 ± 0.0001 Å, respectively. This value is close to the bulk value for $Mn_{0.5}Zn_{0.5}Fe_2O_4$ system (8.4510 Å) [10]. Further, oxygen parameter, u, decreases from sample A to C.

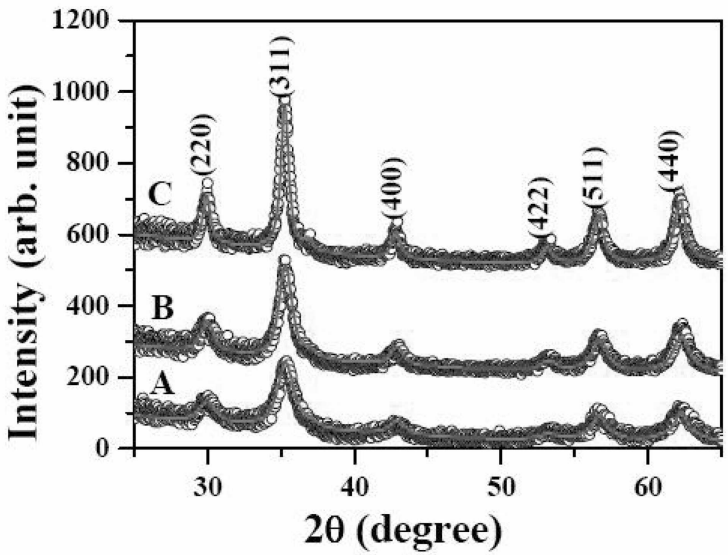

Figure 1. X-ray diffraction patterns for samples A, B and C. The solid line is the Rietveld fitting (see text for more details).

Table 1. Parameters obtained from the Rietveld refinement program.

	Prep. Cond.		X-ray parameters				
Sample	pH	t_d (min)	Zn^{2+} on A-site	D_x (Å) ±3	a (Å) ±0.0001	u (Å)	χ^2
A	10.5	30	0.2	63	8.4495	0.2648	1.44
B	11.6	30	0.5	78	8.4427	0.2620	1.37
C	11.6	60	0.5	137	8.4542	0.2579	1.30

The size of the particles calculated using Scherer's formula for the most intense (3 1 1) reflection plane is 63, 78 and 137 Å for samples A, B and C, respectively (table 1). Increase in pH as well as digestion time lead to increase in particle size that can be explained by the knowledge of the effect of physical and chemical properties of the individual elements used in the system to manipulate the growth of nanoparticles to the desired shape and size [11]. In the typical ferrite system, the critical radius of the nucleated particle size and the structure depend on the pathways from soluble Fe^{3+} and Me^{2+} to thermodynamically stable metal ferrite. With increasing pH, the dissolution of Me^{2+}–Fe^{3+} complexes from the surface takes place followed by crystallization leading to the considerable particle growth, e.g. $(M^{2+}O^{2-})[Fe_2^{3+}O_3^{2-}]$ (where M^{2+} = Mn^{2+}, Zn^{2+}, Co^{2+} etc. except Fe^{2+}), while with increasing digestion time, the Ostwald ripening process dominates where the ions dissolve from the smaller crystals and are deposited on the bigger ones, resulting in the growth of bigger crystals at the expense of the smaller ones.

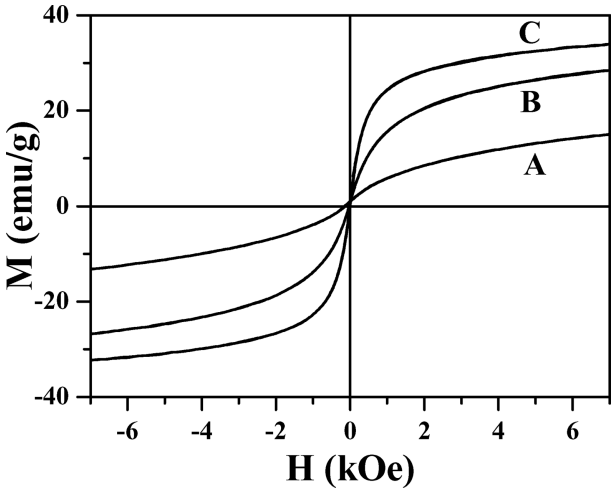

Figure 2. Room-temperature hysteresis loop of particles for samples A, B and C.

4.1.2 *Magnetic properties*

Room-temperature magnetic hysteresis measurements of the powder samples were carried out using EG&G Model 155 vibrating sample magnetometer. The instrument was calibrated with Ni standard. Figure 2 shows the magnetic response of particles to an applied field $[M(H)]$ at 300 K which results from the progressive alignment of an ensemble of magnetic particles. It is inferred from the graph that all the samples exhibit superparamagnetic behaviour, i.e., zero remanence and zero coercivity at 300 K. The superparamagnetic nature of magnetization curve of an assembly of isolated magnetic particles can be manifested by Langevin's theory incorporating with certain assumptions, viz. (i) spherical shape of the particles, (ii) dominance of thermal energy over anisotropy energy, i.e., $KV \ll k_{\mathrm{B}}T$, where k_{B} is the Boltzmann constant, T is the absolute temperature, K is the anisotropy constant and V is the volume of the particle, (iii) polydispersed nature of particles that usually obeys log-normal distribution function and (iv) average domain magnetization, M_{d}, of the particle that remains constant with a given size distribution. In the present case, measurements are carried out on strongly interacting particle system, and therefore, the effect of interparticle interaction is prominent. In the case of interacting superparamagnetic particles having distribution in particle size, Langevin's theory can be modified with mean field theory as [12,13]

$$M = M_{\mathrm{S}} \int_0^\infty f\,(D) L\left(\frac{\mu(H + H_{\mathrm{int}})}{k_{\mathrm{B}}T}\right) \mathrm{d}D, \tag{2}$$

where M_{S} is the saturation magnetization, $L(\alpha) = \coth\alpha - 1/\alpha$ is the Langevin function. The Langevin parameter $\alpha = \mu(H + H_{\mathrm{int}})/k_{\mathrm{B}}T$ where μ is the magnetic moment of individual spin cluster, H is the applied magnetic field, H_{int} (λM_1 where, λ is the mean field constant (dimensionless) and M_1 is the magnetization

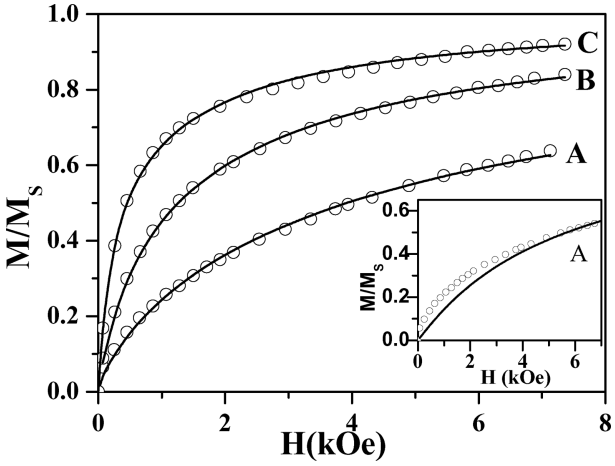

Figure 3. Room-temperature magnetization data for particles fitted with the modified Langevin theory using mean field approximation (eq. (2)). Inset shows the Langevin fitting without mean field approximation.

Table 2. Magnetic parameters derived from the modified Langevin theory (eq. (2)) for particle system.

Sample	D (Å)	σ	λ	M_S (emu/g)
A	62	0.33	60	22.0
B	71	0.33	40	34.5
C	98	0.37	10	36.3

expressed in emu/cc) is the internal field acting on each particle/cluster due to the interaction with other neighbouring particles/clusters which is proportional to the magnetization. Here, $f(D)d(D)$ the log-normal cluster diameter distribution function with mean cluster diameter D_{m} and width σ, can be expressed as

$$f(D)d(D) = \frac{1}{\sqrt{2\pi}\sigma D}\exp\left(\frac{-\ln(D/D_{\mathrm{m}})^2}{2\sigma^2}\right)\mathrm{d}D. \tag{3}$$

Figure 3 shows the virgin curve fitted with eq. (2) where open circles represent experimental data and solid lines represent the calculated data. The fitted parameters are shown in table 2. The mean field constant $\lambda = 60$, 40 and 10 and M_S = 22, 34.5 and 36.3 emu/g for samples A, B and C, respectively, are favoured to represent the observed data well. The goodness of fit is found between 1 and 2 for all the samples. The mean internal field decreases with increasing particle size and M_S. The inset of figure 3 shows fit to the magnetization curve without considering the dipole–dipole interaction.

Low-temperature magnetic hysteresis $M(H)$ loop and temperature-dependent magnetization, $M(T)$, were recorded using quantum design MPMS2 SQUID magnetometer. Figure 4 shows that all the samples are superparamagnetic at 300 K

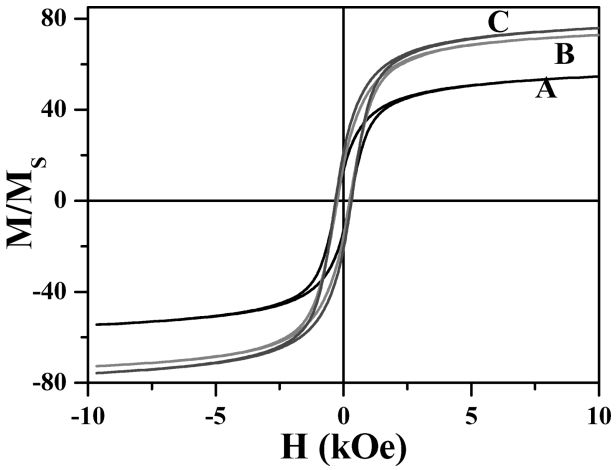

Figure 4. Hysteresis loop of powder samples for A, B and C at 5 K.

Table 3. Parameters derived from the Bloch theory for particle system.

Sample	M_S@5 K (emu/g)	Bloch exponent (α)	Bloch constant $(B)*10^{-4}$	M_S@0 K (emu/g)	T_C (K)	
					M–T	MTG
A	55.0	1.53	1.25	55.0	400	430
B	74.3	1.50	1.20	73.8	411	410
C	78.1	1.50	1.05	78.0	449	450

and possess coercivity at 5 K. The values are 263, 239 and 315 Oe respectively, for A, B and C samples. The saturation magnetization of a system, M_S, determined by extrapolating M vs. $1/H$ curve for high magnetic field region is shown in table 3. It is inferred that the observed saturation magnetization is less than that of the bulk $Mn_{0.5}Zn_{0.5}Fe_2O_4$ ferrite, i.e. 140 emu/g at 5 K. In addition to this, the magnetization loop is open even at 5 K at a given field of 1 T. This non-saturating behaviour is a general feature observed in many nanomagnetic particle systems and can be explained based on the core–shell model [14]. In this model spin at the surface of the particle is considered to be highly disordered, due to either the high surface anisotropy or pinning of the surface spins and required very high field to align these surface spins mixed with ferrimagnetic interactions at the core. By increasing the applied field the ferrimagnetic part tends to saturate whereas the antiferromagnetic part increases linearly resulting in the lack of saturation magnetization. Under this condition if one assumes the bulk saturation magnetization at a given temperature, then the thickness of the surface layer can be expressed by

$$M_S(D) = M_S(\infty)\left(1 - \frac{6t}{D}\right), \tag{4}$$

where $M_S(D)$ represents the saturation magnetization of D-sized particle, $M_S(\infty)$ is the saturation magnetization of bulk samples and t is the thickness of magnetically

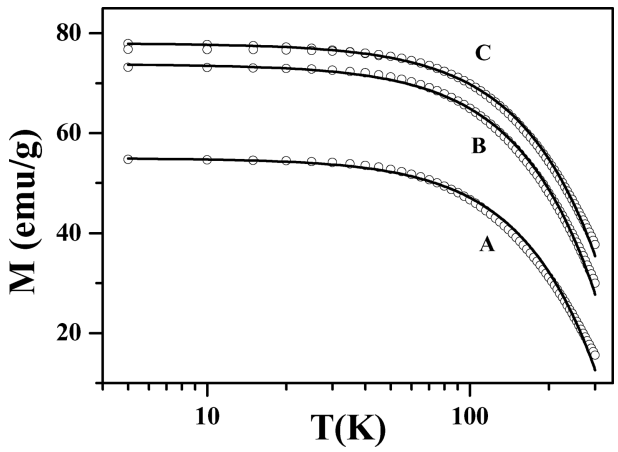

Figure 5. Typical M–T curve fitted with Bloch theory.

dead layer on the particle surface. For sample A, the bulk saturation magnetization at 0 K is calculated as 106.5 emu/g based on the result of cation distribution obtained from Rietveld refinement program, which yields the dead layer thickness as 4 Å, while for samples B and C, the reported bulk saturation magnetization (i.e., 140 emu/g) is used to calculate the thickness and the values are 5.6 and 9.9 Å, respectively.

Thermal behaviour of magnetization was recorded by cooling the substance from 300 K to 5 K in the absence of magnetic field (ZFC) and in the presence of magnetic field (FC). In both cases the data were recorded for warming up the cycle in steps of 5 K. Figure 5 shows typical $M(T)$ curve recorded in the presence of 10 kOe field in ZFC configuration. For temperatures well below the Curie temperature, the temperature-dependent magnetization arises due to the spin-wave fluctuations as described by Bloch, which is given by [14]

$$M(T) = M(0)(1 - BT^{\alpha}), \tag{5}$$

where $M(T)$ is the magnetization at a particular temperature T, $M(0)$ is the magnetization at 0 K, B is the Bloch constant and α is the Bloch exponent. Figure 5 shows fit to the Bloch theory (solid line) fitted with experimental data points. Table 3 represents the fitted parameters. Normally, for the bulk system, Bloch exponent $\alpha = 3/2$. However, in fine-particle system variation in α has been observed. For the present case, it is observed that Bloch exponent comply with bulk system whereas linear decrement in Bloch constant is observed. The Curie temperature (T_{C}) derived from the Bloch constant is almost similar for samples A and B while for sample C increase in T_{C} is observed. The high value of T_{C} for sample C can be explained by considering re-distribution of cations at high temperature and/or due to larger particle size. As discussed earlier in eq. (1), T_{C} strongly depends on the site occupancy of metal ions. In the present system it is assumed that Mn^{2+} ions occupy A-site only whereas the partial presence of Mn^{2+} ion in B-site may change the T_{C} to its original value.

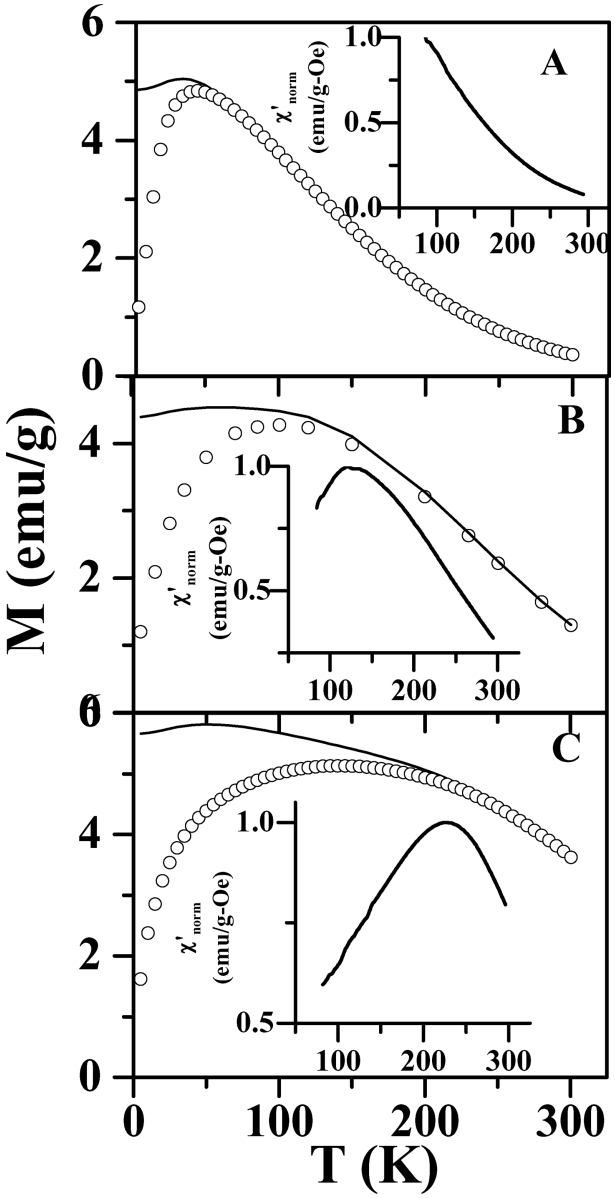

Figure 6. Zero-field-cooled (open circles) and field-cooled (line) magnetization curves for Mn–Zn samples at $H = 50$ Oe. Inset shows the normalized AC-susceptibility curve (real part) taken at 67 Hz frequency.

The low-field temperature-dependent magnetization $M(T)$ for zero-field-cooled (ZFC) and field-cooled (FC) states measured at 50 Oe is shown in figure 6. It exhibits typical superparamagnetic behaviour with a characteristic spin freezing (blocking) temperature T_{B} below which spins are successively locked into the sites

and do not contribute to the overall magnetization. Above T_B, it follows the Curie–Weiss behaviour. The onset of coercivity, i.e., a thermomagnetic irreversibility (T_{irr}) (bifurcation of FC and ZFC curves) is observed at temperature higher than the blocking temperature for all the three samples. In the ideal non-interacting monodispersed system, T_{irr} and T_{max} (maxima in ZFC) occur at the same temperature and are expected to be sensitive to applied DC magnetic field as well as size distribution, because the peak in ZFC shifts towards higher temperature when width increases. Therefore, difference between T_{irr} and T_{max} can be due to the above effect as well as dipole–dipole interaction. In the present case (figure 6), T_B is observed at 45, 100 and 140 K while T_{irr} is observed at around 227, 230 and 260 K for samples A, B and C, respectively. The observed difference in T_{max} and T_{irr} suggests the existence of spin–spin or cluster–spin kind of interactions, along with the particle size distribution – as the present particle system is polydispersed. This type of interaction is expected in highly concentrated nanoparticles system. The peak in ZFC looses its sharpness, becomes rounded and shifts systematically towards high temperature, which can be correlated to the increase in particle size and/or effective anisotropy.

Similar behaviour is also observed in AC susceptibility as a function of temperature carried out at 67 Hz frequency using high precesion custom-built susceptometer [15]. Inset of figure 6 shows the AC susceptibility curves as a function of temperature for all three systems. The figure indicates systematic increase in blocking temperature with increase in size. The blocking temperature of sample A is below 80 K while for samples B and C it is 121 and 228 K, respectively. The difference in blocking temperature between two techniques is attributed to the different time-scales of the measurement.

4.2 *Magnetic fluids*

4.2.1 *Thermogravimetric (TG) and magneto-thermogravimetric (MTG) analysis*

Thermogravimeter (Perkins Elmer-TGS-2) was used to obtain the amount of surfactant bound on the surface of particles. The samples were heated up to 1023 K in inert Ar atmosphere and heating rate was maintained at 20 K per minute. Figure 7 shows the percentage weight loss for the oleic acid coated samples A, B and C as a function of temperature. It is seen that the weight loss in sample B is comparatively less than that observed for samples A and C. The initial weight loss of ∼5% in the range 353–473 K for coated particles may be attributed to desorption of physically adsorbed water molecules, to the weakly bound secondary layer as well as some more weakly bound molecules within the primary surfactant layer. TG curve of all the samples shows one sharp transition, and this suggests desorption of strongly bound primary surfactant layer. This transition is observed at temperature ∼743 K in all the samples indicating that oleic acid completely decomposes at that temperature. No other transition is observed in the TG curve. Therefore, possibility of physi-adsorption of oleic acid molecules are ruled out here. In order to confirm the temperature-induced phase transition, thermogravimetric curve of uncoated particles is recorded. Inset of figure 7 shows typical curves of

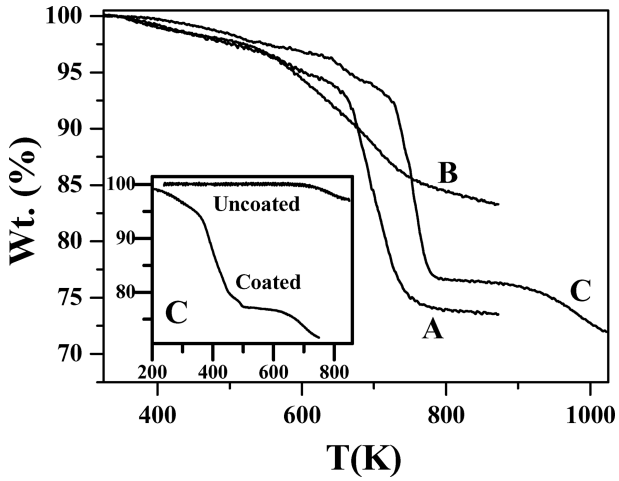

Figure 7. Thermogravimetric pattern for samples A, B and C. Inset shows TG pattern for coated and uncoated particles for sample C.

coated and uncoated particles for sample C. The pattern for uncoated particles is the horizontal line for the entire temperature range of 353 K to 700 K which shows that temperature-induced structural phase transition is not observed in the present system. A similar behaviour for samples A and B is observed. Assuming that the surfactant forms a close-packed monolayer on the nanoparticles, the total weight loss due to the loss of surfactant is calculated theoretically by using the relation [16],

$$\text{Weight loss}(\%) = 100 \frac{\left[\left(\pi D^2/a\right)\left(M/N_0\right)\right]}{(1/6)\,\pi D^3 \rho + \left(\pi D^2/a\right)\left(M/N_0\right)}, \tag{6}$$

where D is the diameter of the magnetic particle, ρ is the density of the magnetic particle, a is the head area of the surfactant attached to particle surface, M is the molecular weight of the surfactant and N_0 is the Avogadro's number. The percentage weight loss for different particle diameters is calculated using eq. (6) with $\rho = 5.170$ g/cc (bulk density), $a = 20$ Å^2 and $M = 282.46$ g/mol (for oleic acid coated particles). The calculated weight loss is 30, 26 and 17% for samples A, B and C, respectively. However, the observed weight loss for samples A, B and C is 25, 15 and 23%, respectively. The observed result is consistent for samples A and C confirming the formation of monolayer coating of surfactant on particle surface which is chemically bound with the particle, while for sample B binding of surfactant molecules is lesser than its monolayer thickness. The difference between theoretical and experimental values can be attributed to polydispersity of the particles, the hindrance effect of surfactant molecules at the interface of small size particles, the shape of the particles (in the calculations, particles are assumed to be spherical though they may not be perfect spheres) and the excess free surfactant molecules available in sample C.

TGA technique was modified to study the change in magnetic phase transition during the measurement, i.e., 'magneto-thermogravimetric' (MTG). In this

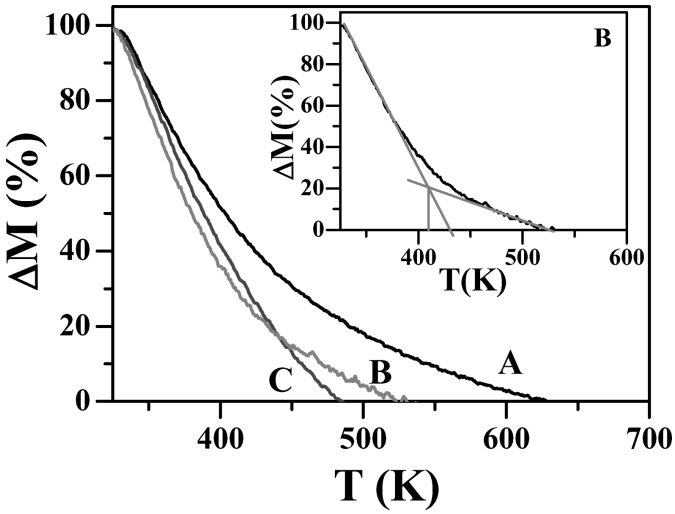

Figure 8. MTG data for samples A, B and C. Inset shows Curie temperature derived from the extrapolation of data points for sample B.

approach an external magnetic field of 150 Oe was applied with permanent magnet to the balance pan of thermogravimetric analyzer containing uncoated particles. Physical weight of the powder sample was set to zero before applying the external magnetic field. In response to the external magnetic field (to the balance pan) the particles get magnetized and hence new reading of weight appears which depends on the magnetic properties of the particle. In order to record the temperature-dependent change in magnetization, new magnetic weight of the sample was set to maximum and the temperature was raised to 1023 K at 20 K/min rate.

Figure 8 shows the percentage change in magnetization as a function of temperature for all the samples. Since the physical weight is tare off and magnetic weight is set as maximum, the reduction in the weight loss can be correlated to the change in magnetic moment with temperature. The observed single step transition within the entire temperature range indicates magnetically single phase (figure 8). Additionally, change in rate of magnetization is different in all the three samples which can be attributed to the variation in particle size and/or cation distribution. Curie temperature of the system can be retrieved by cross-over point of the line drawn from the initial rate of change in magnetization at low temperature and paramagnetic contribution at high temperature (assuming linear variation). This is because particles are ferrimagnetic from room temperature to its Curie temperature and above Curie temperature they behave as paramagnetic. Hence the response of particles below and above Curie temperature is different which resulted in a change in slope in data. Figure 8 (inset) shows typical curve for sample B with extrapolated line – indicating T_C of the sample. The value of Curie temperature thus obtained is reported in table 3. The extrapolated T_C value of sample A is slightly higher than the value obtained from the Bloch theory. In samples B and C, the deduced T_C matches with that obtained from SQUID measurements. The present results indicate that the MTG technique can be used to determine Curie temperature of NMP and also to study magnetic phase transition at high temperature.

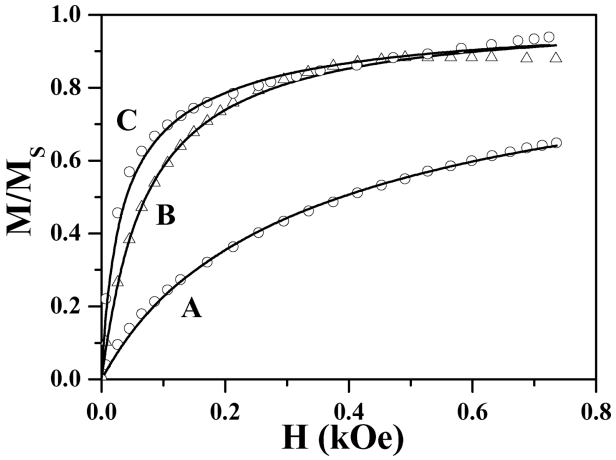

Figure 9. Room-temperature magnetization data of magnetic fluids (open circle) fitted with modified Langevin theory (solid line).

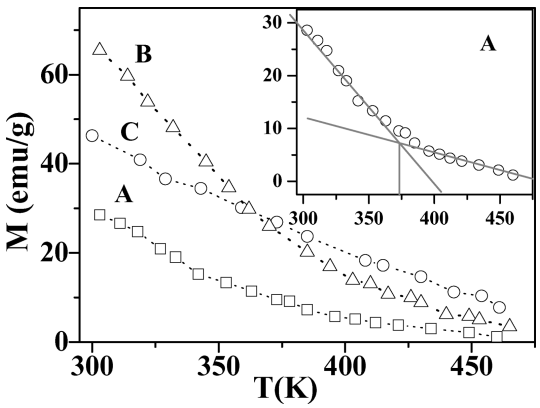

Figure 10. High-temperature magnetization measurements for all three magnetic fluid samples. Inset shows determination of Curie temperature for sample A using extrapolation of data points.

4.2.2 *Magnetic properties*

To record the magnetization data of magnetic fluid at high temperature a home-built magnetometer was used. The data were recorded in the temperature range of 300 K to 573 K for a fixed field of 1.2 kOe. The set-up was calibrated with a standard fluid of known value of magnetization.

Figure 9 shows the normalized magnetic response (M/M_S) for all three fluid samples at room temperature (300 K). The experimental data (open symbol) are fitted with the Langevin theory for non-interacting system ($\lambda = 0$). The magnetic parameters derived from the fit are shown in table 4. The value of goodness of fit

Table 4. Magnetic parameters derived from the Langevin theory for magnetic fluid system.

Sample	M_d (emu/cc)	D (Å)	σ	T_C (K)
A	132	65	0.40	370
B	170	95	0.32	370
C	210	92	0.52	443

between 1 and 2 shows best fit of experimental data with eq. (2) for all three samples. It is evident from the figure that magnetic response increases systematically from sample A to C. This is due to the enhancement in domain magnetization of the particle with increase in particle size from sample A to sample C. It is known that the larger size particles will respond more to the lower field strength compared to smaller size particles. Therefore, the overall magnetic response increases with increasing particle size. Further, the value of domain magnetization of the particle obtained for the fluid is in good agreement with that obtained from the particle magnetization (see table 2).

In order to determine the Curie temperature of the particles dispersed in magnetic fluid, the temperature-dependent magnetic measurements are carried out. Figure 10 shows the change in magnetization as a function of temperature at a constant field strength of 1.2 kOe. The Curie temperatures of the magnetic fluid thus obtained are shown in table 4. It is observed that T_C increases from sample A to C which is consistent with the trend observed in the case of particle but the value of T_C is lower in the case of fluid.

5. Conclusion

Three different samples of $Mn_{0.5}Zn_{0.5}Fe_2O_4$ ferrite particles were synthesized under controlled conditions using hydrothermal technique. Rietveld refinement of the XRD pattern reveals the formation of single phase spinel structure. The cation distribution obtained from the fit shows the presence of Zn ion on both the sites (A and B) in sample A while for samples B and C it remains on A-site only. $M(H)$ loop at room temperature indicates superparamagnetic nature with non-saturating behaviour in an applied field of 7 kOe. Modified Langevin's theory by incorporating the interparticle interaction was used to fit the virgin curve of particle magnetization. It is observed that mean field constant decreases with increasing particle size and saturation magnetization. Low-temperature magnetization behaviour follows Bloch spin wave theory. The Curie temperature derived from the Bloch constant increases from 400 to 450 K with increase in particle size from 54 to 135 Å, respectively. The Curie temperature is also obtained from modified thermogravimetric method and high-temperature fluid magnetization and the results are in agreement with each other.

Acknowledgement

Authors acknowledge Prof. K V Rao and Dr Lyuba Belova, Tmfy-MSE, Royal Institute of Technology (RIT), Sweden for providing experimental facilities. KP acknowledges DST, New Delhi for BOYSCAST fellowship to work at Tmfy-MSE, Royal Institute of Technology (RIT), Sweden. VD acknowledges CENNP (Gujarat Council of Science & Technology – GUJCOST, India) for providing financial support in term of fellowship. RD acknowledges Tmfy-MSE for financial support.

References

[1] J Wang, Q Chen, C Zeng and B Hou, *Adv. Mater.* **16**, 137 (2004)
[2] V F Puntes, K M Krishnan and A P Alivisatos, *Science* **291**, 2115 (2001)
[3] C Petit, A Taleb and M P Pileni, *J. Phys. Chem.* **B103**, 1805 (1999)
[4] A G Roca, M P Morales, K O'Grady and C J Serna, *Nanotechnology* **17**, 2783 (2006)
[5] X Tang and H Yang, *Nanotechnol.* **16**, S554 (2005)
[6] H Matsuki and K Murakami, *J. Magn. Magn. Mater.* **65**, 363 (1987)
[7] K Nakatuska, Y Hama and J Takahashi, *J. Magn. Magn. Mater.* **85**, 207 (1990)
[8] M A Gilleo, *Phys. Rev.* **109**, 777 (1958)
[9] A Brose van Groenou, P F Bongers and A L Stuyts, *Mater. Sci. Eng.* **3**, 317 (1968)
[10] J Smit and H P J Wijn, *Ferrites* (Wiley, New York, 1959) p. 158
[11] G Gnanaprakash, John Philip and Baldev Raj, *Mater. Lett.* **61**, 4545 (2007)
[12] B D Cullity, *Introduction to magnetic materials* (Addison Wesley, Reading, 1972)
[13] M D Mukadam, S M Yusuf, P Sharma and S K Kulshreshtha, *J. Magn. Magn. Mater.* **269**, 317 (2004)
[14] J P Chen, C M Sorensen, K J Klabunde, G C Hadjipanayis, E Delvin and A Kostikas, *Phys. Rev.* **B54**, 9288 (1996)
[15] S Valter, Ph.D. Thesis (Royal Institute of Technology, Sweden, 1998)
[16] P J Van der Zaag, J J M Ruigrok, A Noordermeer, M H M W van Delden, P T Por, M Th Rekveldt, D M Donnet and J N Chapman, *J. Appl. Phys.* **74**, 4085 (1993)